AN ABSTRACT OF THE THESIS OF

Ajax Barros De Melo (Name) for the Master of Science (Degree)

in Electrical and Electronics Engineering (Major) presented on July 30, 1971 (Date)

Title: STUDIES ON ATTITUDE CONTROL OF SMALL PAYLOADS OF SOUNDING ROCKETS

Redacted for Privacy

Abstract approved: S. A. Stone

This work has the purpose of presenting an approach to attitude control applicable for sun alignment on scientific payloads.

As a primary source of information in order to obtain the alignment error signals, four solar cells are disposed about the body of the payload. As a secondary source a pair of magnetometers are used.

In the development of this thesis, the author stresses some approximations useful for the sake of simplicity without compromising the results. He points out several technological aspects which are necessary for practical realization of the system.

The theory of fluxgate magnetometers is discussed and a model for the simulation of the sensor is given.

Every step of development presents a model for a further simulation of the system.

Studies on Attitude Control of Small Payloads of Sounding Rockets

by

Ajax Barros de Melo

A THESIS

submitted to

Oregon State University

in partial fulfillment of
the requirements for the
degree of

Master of Science

June 1972

APPROVED:

Redacted for Privacy

Professor of Electrical and Electronics Engineering

in charge of major

Redacted for Privacy

Head of Department of Electrical and Electronics Engineering

Redacted for Privacy

Dean of Graduate School

Date thesis is presented July 30, 1971

Typed by Barbara Eby for Ajax Barros de Melo

ACKNOWLEDGMENT

The author extends his thanks and appreciation to his major professor Professor S. A. Stone for his many helpful suggestions and encouragements in the preparation of this dissertation. Also I wish to acknowledge Professor C. E. Smith for critically reading the manuscript. Special thanks goes to my wife, Ismenia, for without her help and patience this work could not have been completed.

TABLE OF CONTENTS

LIST OF FIGURES

LIST OF TABLES

STUDIES ON ATTITUDE CONTROL OF SMALL PAYLOADS OF SOUNDING ROCKETS

I. INTRODUCTION

One of the requirements considered in any engineered device for research is its cost. This must be minimized to accomplish a desirable degree of optimization and is a function of several variables.

Experiments carried on using unstabilized payloads include meteorological and acoustical research with sounding granades, ionospheric and tropospheric ion counters, total field magnetometers, etc.

Many upper atmosphere experiments are orientation-sensitive and in stabilized experiments we can do: Soft x-rays and ultraviolet source detection, stellar photometry, and several types of dispersion spectroscopy. These experiments sometimes must be stabilized by automatic pointing systems.

After reviewing various methods of obtaining attitude data, it became clear that an instrumentation which is able to measure the solar angle and the orthogonal components of the geomagnetic field has advantages in simplicity and cost. Gyros and associated devices are expensive, complex, and require a reasonable amount of ground adjustments.

This paper has considerations about the development of a sun-oriented attitude control system that avoids the use of gimbaled devices, accelerometers, and more sophiscated attitude sensors.

Attitude control is defined as control of the rotational motion or orientation of the spacecraft about its center of mass. Also, this term is usually used in connection with the unpowered or coasting phase of a mission. A final function performed by spacecraft control systems is that of moving or pointing articulating members such as antennas, sensors, cameras in the proper direction.

In order to accomplish the proper control there are several different classes of actuators which are used in attitude control systems. Typical torques required of these actuators are 1.5 to 20 ft-lb (D. M. Chisel, R. K. Rose, 1968). The first and probably most common class of actuators for attitude control includes the mass-expulsion devices. The working fuel is stored in the spacecraft, and a small quantity is expelled from the spacecraft in the proper direction whenever it is desired to apply a torque to the vehicle. The fuel stored for this purpose may be gas, liquid which is decomposed into vapor, liquid which burns directly in a combustion chamber of a thrustor, or a subliming or decomposing solid.

A second class of actuators is the momentum exchange devices. To obtain a control torque, the spacecraft reacts against a wheel or sphere. Hence, momentum from the spacecraft is transferred to the

reaction element. The net angular momentum of the spacecraft system including the reaction device does not change during this operation. Momentum exchange devices have been successfully used in satellites where the disturbing torques are cyclical; however, for undirectional disturbance torques the speed of the reaction wheel or sphere will continue to increase to dangerous speeds. In this case some other elements must be used to desaturate the reaction element. (9)

Another class of actuators is the field effect devices (3). This class includes those which interact with magnetic, gravitational (11), and/or solar radiation fields to produce useful control torques. These actuators are somewhat limited in their application because they are capable of producing only a very small torque.

Considering the above and the fact that the time of flight of a sounding rocket experiment is short when compared with a satellite mission, the simplest means of orienting a payload is by placing pairs of mass-expulsion devices about each of the control axes.

II. SYSTEM CONFIGURATION

The attitude system studied will be used on small spin-stabilized vehicles, with payload separation from the sustainer after its burnout.

For the purpose of this study only the payload will be stabilized, avoiding the complexities of the mathematical models which describe the dynamical behavior of the rocket during the first part of its trajectory. In this way, aerodynamics effects, fuel sloshing, atmospheric randon perturbations, and parameters concerned with the vector will not be considered.

Figure 1 shows a typical configuration for a stabilized payload. Figure 2 shows the sequence of events which are normal in stabilized experiments.

Our system may be described as a sun-oriented attitude control system in which sun sensors have been chosen as a primary source of control information. The attitude with respect to the third axis is given by two flux-gate magnetometers. The control starts at the instant of the payload separation from the rocket. Gas jets despin the payload through control signals given by the magnetometers and the lateral coarse sun sensors.

When the spin signal falls below a pre-selected threshold, the attitude error about the third axis is used for the sun line acquisition.

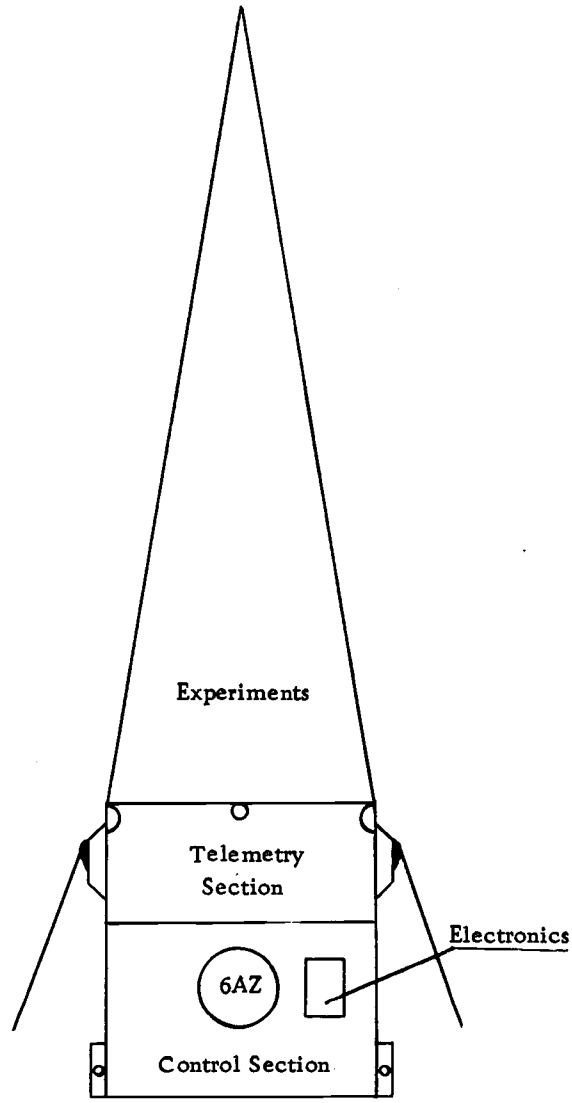

Figure 1. Configuration of a stabilized payload.

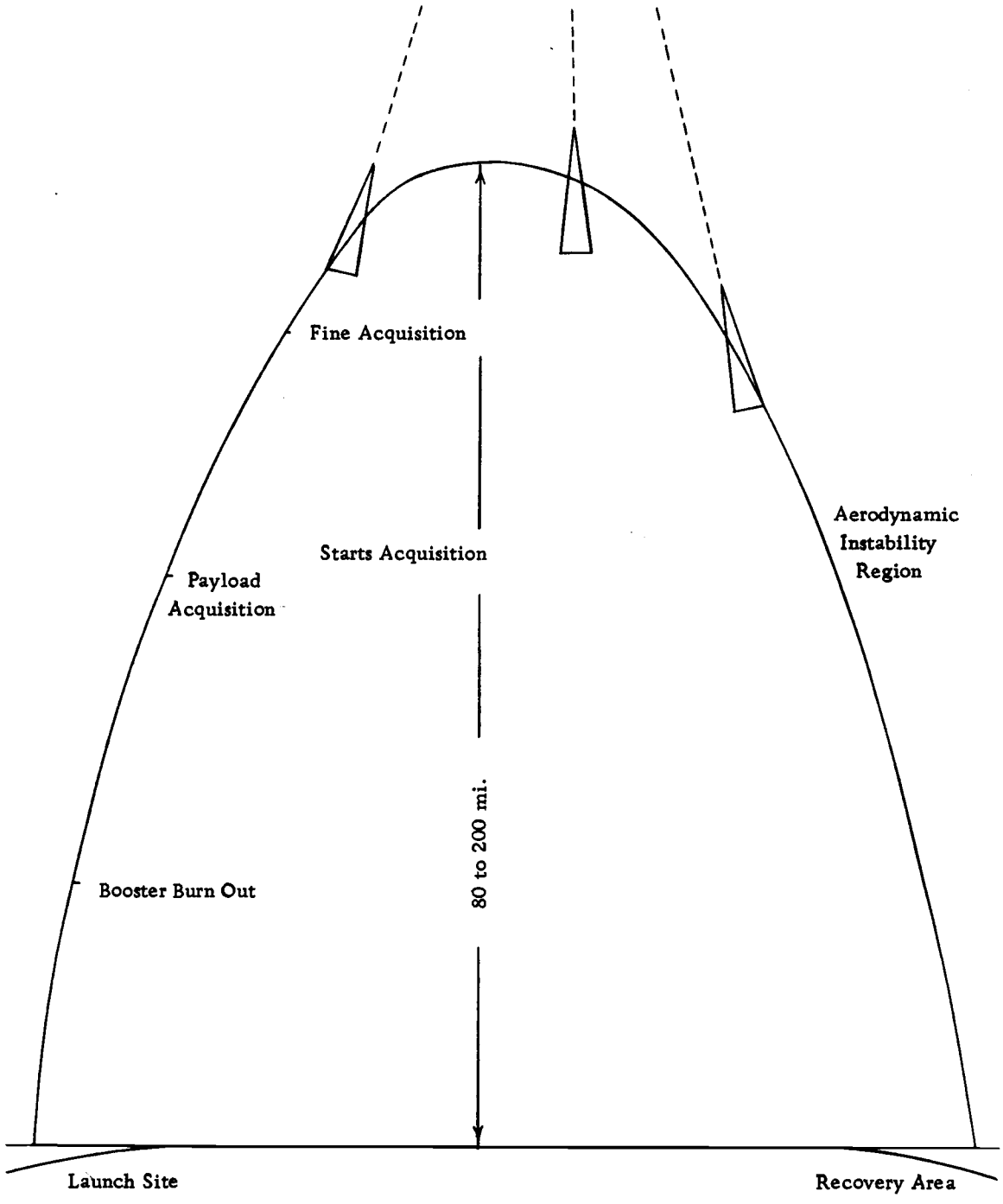

Figure 2. Sequence of events of a stabilized experiment.

Magnetometer and the sun sensor outputs are summed and demodulated in order to feed the control gas valves.

If we use a lateral solar sensor which has a square root output with respect to the solar misalignment angle and a linear output of the magnetometer, the combination produces a parabolic phase plane switching boundary (17). The acquisition time is then optimized. The precession signal is obtained by the differentiation of the coarse sensor and the Z-axis magnetometer output. When the payload and rocket are separated, the control sequence is divided into two parts: First, payload despin and solar acquisition utilizes a direction cosine approach; Second, fine pointing utilizes the fine sun sensor.

For equatorial launchings of interest here, it is noticed that the output of the magnetometer aligned with the longitudinal axis of the payload gives a small asymmetry for small values of the precession angles. This is the case since at these latitudes the inclination angle of the geomagnetic field is small.

In general when we need to obtain the spin information as well as the precession angle, we use two magnetometers, one aligned with the longitudinal axis of the payload and the other at $\tilde{1}1/2$ rad with respect to the first sensor.

Studies made by J. A. A. Amarante (2) and G. R. Young and J. D. Timmons (31) show it is possible to use only one magnetometer with an inclination between 20^{o} and 30^{o} with respect to the principal

payload axis. With this solution we have to allow a certain amount of imprecision in the obtained attitude data.

The equations in this paper will be developed considering the despin and acquisition phases (16).

III. DERIVATION OF THE EQUATIONS OF CONTROL

Upon a superficial examination it would appear that the selection of appropriate reference frames for a payload in the unpowered phase of the flight is straightforward. Using a conventional system of reference, defined by the solar and geomagnetic local field vectors and considering that these two vectors must not be coincident with an angle between them assumed to lie in the range 30° to 150° (17), we can define the control law for the pitch and yaw axes as the parallelism of two axes: the spin axis and the main solar axis. In order to accomplish the above we can define initially two sets of coordinates systems: i_1, i_2, i_3 and e_1, e_2, e_3 respectively the payload fixed frame and the solar coordinate axes (Figure 3).

The control law for the pitch and yaw axis is:

$$\vec{i}_1 \times \vec{e}_1 = 0 \tag{1}$$

An additional term will appear to account for the roll control:

$$\vec{i}_3 \times \vec{e}_3 = 0 \tag{2}$$

The axis i_3 would always be coincident with the $\vec{e}_3$ when the control law is satisfied. A new vector is defined which is free to rotate in the plane i_3, i_2 (Figure 4). Using Figure 4a where M_{123} is the magnetic coordinate system and m_{ij} are the direction cosines

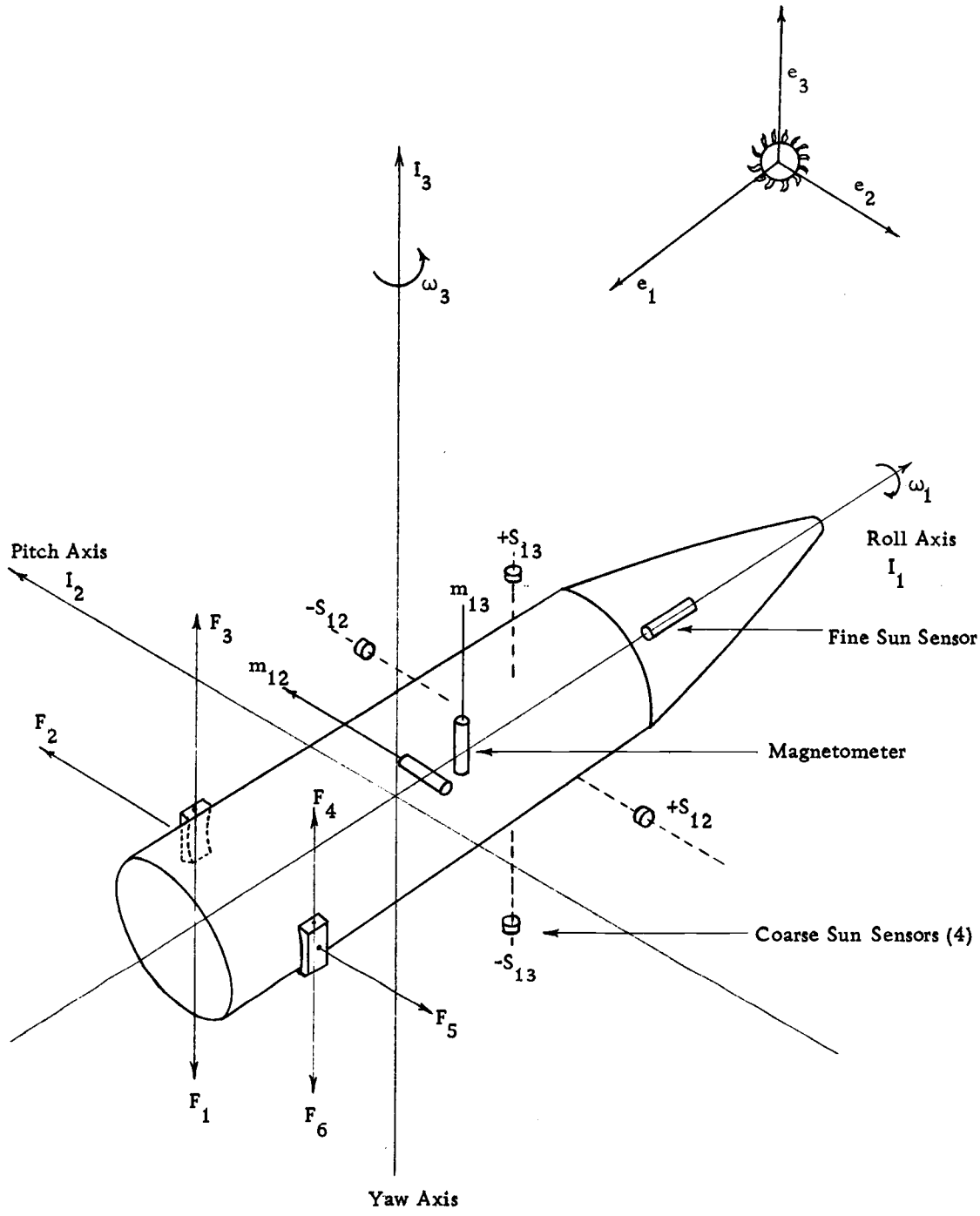

Figure 3. Sensor locations with respect to the coordinate axes.

between the vehicle and the magnetic system, we define the new vector $\vec{3g}$ which is the roll null axis as:

$$\vec{3g} \times \vec{e_3} = (\vec{i_3} \cos\phi_i + \vec{i_2} \sin\phi_i) \times \vec{e_3} = 0$$

The roll angle which satisfies the control law, is determined by ϕ_i according to Figure (4).

In order to satisfy the control law a torque proportional to the attitude error must be applied:

$$T_c = K_1(\vec{i_1} \times \vec{e_1}) + K_2\{(\vec{i_3} \cos\phi_i + \vec{i_2} \sin\phi_i) \times \vec{e_s}\} \qquad (4)$$

where K_1 and K_2 are constant gains chosen to optimize the system.

The transformation between the vehicle and the solar reference axis is

$$\begin{pmatrix} \vec{e_1} \\ \vec{e_2} \\ \vec{e_3} \end{pmatrix} = \begin{pmatrix} S_{11} & S_{12} & S_{13} \\ S_{21} & S_{22} & S_{23} \\ S_{31} & S_{32} & S_{33} \end{pmatrix} \begin{pmatrix} i_1 \\ i_2 \\ i_3 \end{pmatrix} = (S) \begin{pmatrix} i_1 \\ i_2 \\ i_3 \end{pmatrix} \qquad (5)$$

The torques can be written in component form:

$$\begin{aligned} T_{roll} &= K_2(S_{33} \sin\phi_i - S_{32} \cos\phi_i) \\ T_{pitch} &= -K_1 S_{13} - K_2 S_{31} \cos\phi_i \\ T_{yaw} &= K_1 S_{12} - K_2 S_{31} \sin\phi_i \end{aligned} \qquad (6)$$

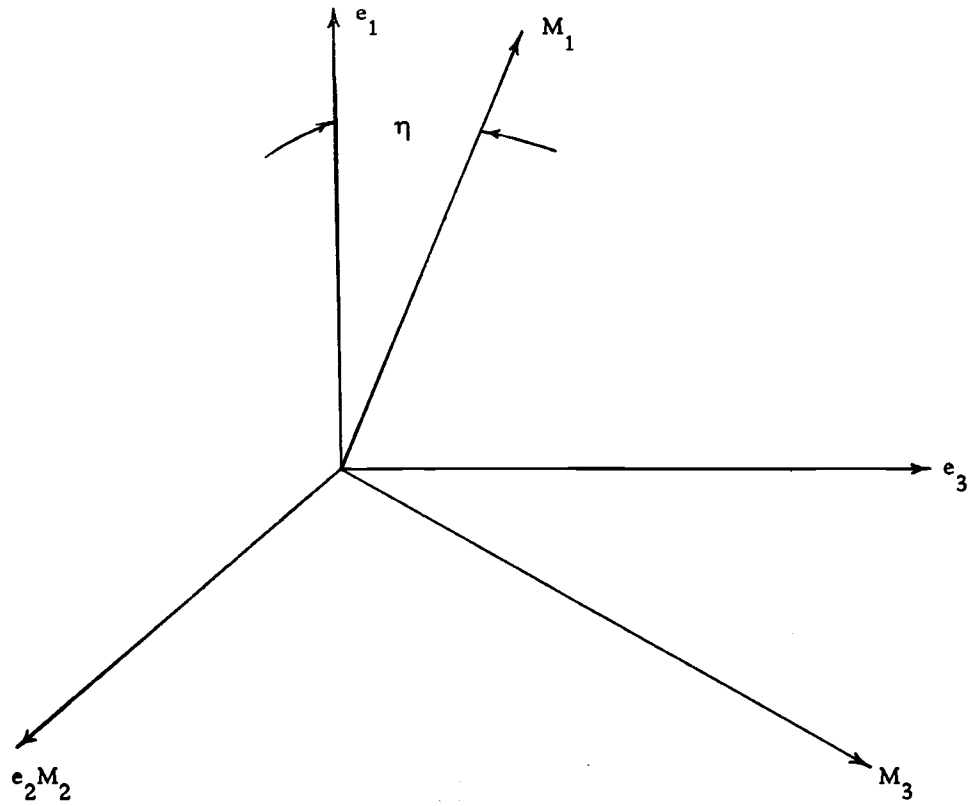

Figure 4a. Payload coordinate system.

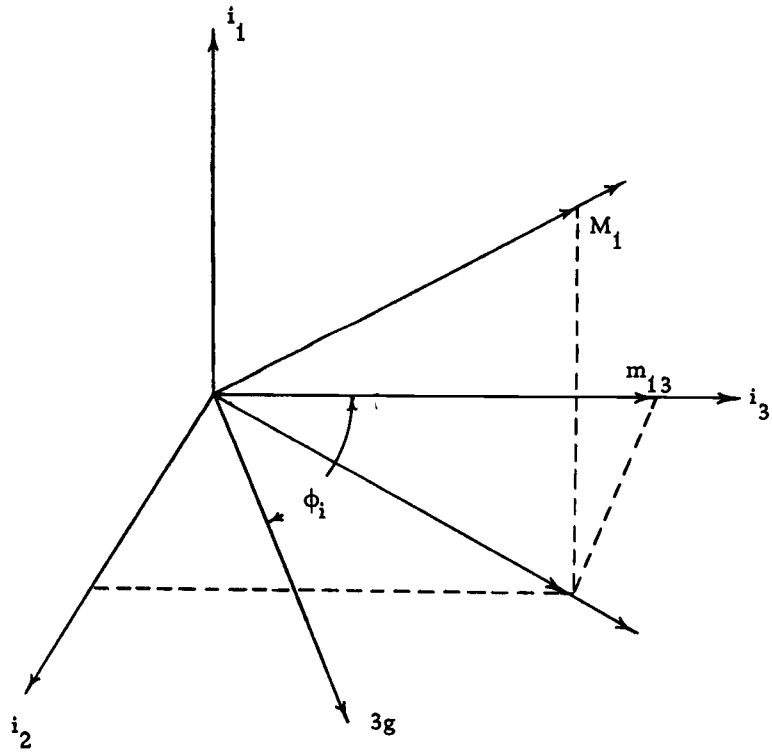

Figure 4b. Roll command angle ϕ_i.

We can achieve some simplifications if we consider that when the attitude error about a given axis is zero the corresponding control torque will be zero, regardless of the error about other axis. In Equation (6), S_{13} is a measure of the pitch error for some roll attitude and if S_{13} is zero T_p will also be zero, since the pitch component of the Equation (1) is satisfied. The $K_2 S_{31}$ comes from the roll part of the control law and if nonzero, it will cause T_p to be nonzero even though S_{13} is zero. Consequently, this term is neglected along with the similar term in the T_y equation. These simplifications were checked by analog computer methods and air-bearing tests by Q. M. Hansen et al. (1967).

If we added damping for stability, the control moment equations becomes:

$$\begin{aligned} T_r &= -K_2(S_{32}\cos\phi_i - S_{33}\sin\phi_i) + \text{roll damping} \\ T_p &= -K_1 S_{13} + \text{pitch damping} \\ T_y &= +K_1 S_{12} + \text{yaw damping} \end{aligned} \tag{7}$$

The terms S_{12} and S_{13} are direction cosine terms between the solar vector and the vehicle i_2 and i_3 axes respectively. Since the output of the solar cell has a square root output with respect to the angle of incident light, S_{12} and S_{13} may be measured as a square root of the solar cell output signal.

The terms S_{32} and S_{33} are direction cosines between the e_3 coordinate axis and the i_2, i_3 axes respectively. These quantities cannot be measured directly but it can be shown that by the use of suitable transformation, unmeasurable variables can be replaced by others which can easily be sensed. In our case, S_{32} and S_{33} may be computed from the output of the magnetometer and sun sensor.

The transformation between the payload axis and the magnetic axis is:

$$\begin{pmatrix} M_1 \\ M_2 \\ M_3 \end{pmatrix} = \begin{pmatrix} m_{11} & m_{12} & m_{13} \\ m_{21} & m_{22} & m_{23} \\ m_{31} & m_{32} & m_{33} \end{pmatrix} \begin{pmatrix} i_1 \\ i_2 \\ i_3 \end{pmatrix} = (M) \begin{pmatrix} i_1 \\ i_2 \\ i_3 \end{pmatrix} \quad (8)$$

Solar and magnetic coordinate axes are related by η rotation about $e_1 M_2$ axis (Figure 4).

$$\begin{pmatrix} M_1 \\ M_2 \\ M_3 \end{pmatrix} = \begin{pmatrix} \cos & 0 & -\sin \\ 0 & 1 & 0 \\ \sin & 0 & \cos \end{pmatrix} \begin{pmatrix} e_1 \\ e_2 \\ e_3 \end{pmatrix} = (\eta) \begin{pmatrix} e_1 \\ e_2 \\ e_3 \end{pmatrix} \quad (9)$$

Combining Equations (5), (8) and (9)

$$(\eta)(S) = (m) \quad (10)$$

and solving for the S_{3j} terms we find:

$$S_{31} = (S_{11}\cos\eta - m_{11})/\sin\eta$$

$$S_{32} = (S_{12}\cos\eta - m_{12})/\sin\eta \qquad (11)$$

$$S_{33} = (S_{13}\cos\eta - m_{13})/\sin\eta$$

Since m_{11}, m_{12}, m_{13} are the direction cosines between the magnetic field vector and the vehicle coordinate axes, they may be measured by the magnetometer. As the S_{32} and S_{33} are expressed in terms of measurable components, the roll component of the control law is:

$$\text{-Roll damp} + T_{roll}$$

$$= (-K_2/\sin\eta)\{(S_{12}\cos\eta - m_{12}\cos\phi_i) - (S_{13}\cos\eta - m_{13})\sin\phi_i\} \qquad (12)$$

The damping signals are provided by rates computed from the direction cosines output of the sun sensor and the magnetometer. They are derived by differentiating Equation (5) and noting that $\dot{e}_1=\dot{e}_2=\dot{e}_3=0$ since these reference axes constitute an inertial reference system.

$$\omega_1 = \dot{S}_{12}S_{13} + \dot{S}_{22}S_{23} + \dot{S}_{33}S_{33}$$

$$\omega_2 = \dot{S}_{13}S_{11} + \dot{S}_{23}S_{21} + \dot{S}_{33}S_{31} \qquad (13)$$

$$\omega_3 = -\dot{S}_{12}S_{11} - \dot{S}_{22}S_{21} - \dot{S}_{32}S_{31}$$

The S_{1j} terms may be directly measured by solar cells. The expression for the S_{3j} terms are derived in Equation (11). However the S_{2j} terms must be computed. From the Figure (5a), $\vec{e}_2=\vec{e}_3 \times \vec{e}_1$.

When substitutions are made from Equation (5) the results are:

$$S_{21} = S_{32}S_{13} - S_{33}S_{12}$$

$$S_{22} = S_{33}S_{11} - S_{31}S_{13}$$

$$S_{23} = S_{31}S_{12} - S_{31}S_{11}$$

The equations of control which give us the control error will be:

$$\delta_r = (K_2/\sin\eta)\{(S_{12}\cos\eta - m_{12})\cos\phi_i - (S_{13}\cos\eta - m_{13})\sin\phi_i\} - h_1\omega_1$$

$$\delta_p = -K_1S_{12} - h_3\omega_3$$

$$\delta_y = K_1S_{12} - h_3\omega_3$$

Where h_1, h_2, and h_3 are constants.

We replaced the T's of Equations (7) and (12), since the control torques will be applied to the payload as a function of δ's.

Considering Figure (5), control torques may be defined as the reaction of six nozzles arranged as shown. Then:

$$\begin{aligned} T_{roll} &= (F_1 + F_4) \text{ or } -(F_3 + F_6) \\ T_{pitch} &= (F_3 + F_4) \text{ or } -(F_1 + F_6) \\ T_{yaw} &= (F_5 \text{ or } -F_2) \end{aligned} \qquad (16)$$

The error parameters will be applied following the expressions:

$$\begin{aligned} F_1 &= K_r\delta_r + K_p\delta_p = -F_3 \\ F_4 &= K_r\delta_r - K_p\delta_p = -F_6 \\ F_2 &= -K_y\delta_y = -F_5 \end{aligned} \qquad (17)$$

Observing Equation (15) we can see that the term $h_1\omega_1$ is predominant in δ_r during the despin phase of orientation, and δ_r predominates over δ_p in Equation (17).

Another interesting observation is that, when δ_p affects the acquisition, the payload sun angle has been reduced so that pitch motion occurs in a plane and the parameter ω_2 is approximately equal to S_{13}. This allows the circuitry necessary to compute ω_2 to be replaced by a lead network.

The pulses from the yaw nozzle are used for precession corrections and these corrections are sensitive to ω_1. Then the yaw jets should be commanded by a precession signal proportional to $\omega_1 S_{13} = S_{12}$. It follows that if ω_3 is replaced by S_{12} the precession signal is available during despin and by the same arguments for δ_p, S_{12} is also the proper yaw channel damping signal during the acquisition.

We can notice in the equation of roll error that the term containing m_{12} and m_{13} predominate during the fine pointing ($S_{12}, S_{13} \rightarrow 0$). When S_{12}, S_{13} are eliminated, the roll position signal will be degraded from the completion of despin until S_{12} and S_{13} become small. Also when we eliminate S_{12}, S_{13}, the resulting will be that η appears only as a constant gain in the form of $\frac{1}{\sin\eta}$. Since we state that $30^\circ \leq \eta \leq 150^\circ$ and $1 \leq \frac{1}{\sin\eta} \leq 2$ the roll loop gain varies 2 to 1. If we assign a nominal value of 30° for η the roll equation becomes:

$$\delta_r = \left(\frac{K}{2}\right)\left(m_{12}\cos\phi_b - m_{13}\sin\phi_b\right) - h_1\omega_1 \qquad (18)$$

Now using the approximations given in the appendix of reference (17)

$$\dot{S}_{13} = -\omega_1 S_{12} \qquad \dot{m}_{12} = \omega_1 m_{13} \qquad \dot{m}_{13} = -\omega_1 m_{12}$$

and noting that

$$S_{12(\mathrm{sgn}S_{13})} = \omega_1 S_{13}(\mathrm{sgn}S_{13}) = \omega_1 |S_{13}|$$

and similar expression, we obtain the expression for ω_1

$$S_{12}(\mathrm{sgn}S_{13}) - S_{13}(\mathrm{sgn}S_{12}) + m_{12}(\mathrm{sgn}m_{13}) - m_{13}(\mathrm{sgn}m_{12})$$

$$= \omega_1 [(|S_{13}| - |S_{12}| + |m_{13}| - |m_{12}|)]$$

The matrix S can be written in terms of the Euler angles as:

$$S = \begin{pmatrix} C\theta C\Psi & C\theta S\Psi & -S\theta \\ (S\phi S\theta C\Psi - C\phi S\Psi) & S\phi S\theta S\Psi + C\phi C\Psi & S\phi C\phi \\ C\phi S\theta C\Psi + S\phi S\Psi & C\phi S\theta S\Psi - S\phi C\Psi & C\phi C\theta \end{pmatrix}$$

Where C = cos and S = sin.

IV. DERIVATION OF THE PAYLOAD EQUATIONS

The analytic considerations relative to spinning rockets with respect their dynamic behavior exhibit many of the characteristics of gyroscopes.

The symmetry axis of a spinning, axially symmetrical body will execute a conning motion when free from external torques. This motion as observed for free spinning rockets, has the rocket spin axis sweep out the surface of a cone in space. In spite of the fact that in this case is often referred to as free precession this motion is actually nutation. The conning motion occurs when torques are removed on the spinning rocket.

The quantitative description of a spinning rocket dynamics effect can be accomplished by generating and solving the equation of motion of a spinning, cylindrically-shaped rigid body (12).

In our case, we will derive the equation of a spinning payload which has attained a sufficiently high altitude in order to be free of the atmospheric aerodynamic effects.

The total angular momentum vector of the system is conserved and can be divided into two components: One along the spin axis and other on the direction of the transverse axis with respect to the first.

As a nonzero transverse component of total angular momentum is present, the total angular momentum vector does not lie along the

vehicle spin axis. Consequently, the spin axis precesses around the total angular momentum vector since this vector must remain fixed relatively to the free falling reference frame. This condition of free conning will persist until external torque be applied.

Assuming the spin rate constant and the pitch and yaw angles lying in a range not greater than 40^{o}, we can describe the motion of a rigid body by a set of linear differential equations.

Writing those equations in terms of pitch and yaw we find:

$$\begin{aligned} I\ddot{\theta} + H\dot{\psi} &= T_{pitch} \\ I\ddot{\psi} - H\dot{\theta} &= T_{yaw} \\ I\ddot{\theta} &= T_{roll} \end{aligned} \tag{19}$$

Solving the above system of equations only in terms of pitch and yaw we find:

$$\theta = \theta_0 - \frac{T_{yaw}t}{H} + (\frac{\dot{\theta}_0}{p} + \frac{T_{yaw}}{H_p})\sin(pt) + (\frac{T_{pitch}}{Hp} - \frac{\psi}{p})[1 - \cos(pt)]$$

$$\psi = \psi_0 - \frac{T_{pitch}t}{H} + (\frac{\dot{\psi}_0}{p} - \frac{T_{pitch}}{Hp})\sin(pt) + (\frac{T_{yaw}}{Hp} + \frac{\dot{\theta}_0}{p})[1 - \cos(pt)] \tag{20}$$

Where $(\theta_0 - \frac{T_{yaw}t}{H})$ and $(\psi_0 + \frac{T_{pitch}}{H})$ are regular precession terms and the rest of the equation terms are nutation terms. In the equation above, H is the spin angular momentum, T_{yaw} is the i_2 and i_3 components of the impressed torque, p is identified as p=H/I where

I is the transverse moment of inertia. The factor p is the nutation frequency.

Precession with zero nutation is possible since the impressed control torque and the initial conditions satisfy the following equations:

$$\begin{aligned} [\dot{\theta}_0 + \frac{T_{yaw}}{H}] &= 0 \\ [\frac{T_{pitch}}{H} - \dot{\psi}_0] &= 0 \end{aligned} \tag{21}$$

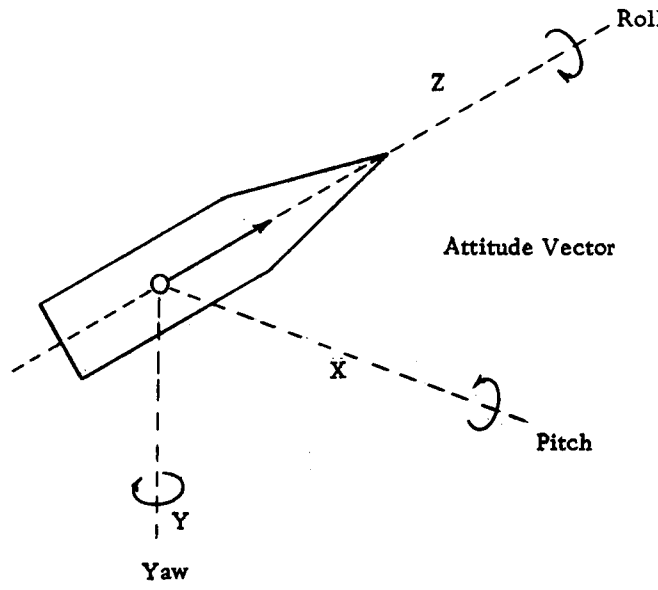

Figure 5. Principal axes of a spinning payload.

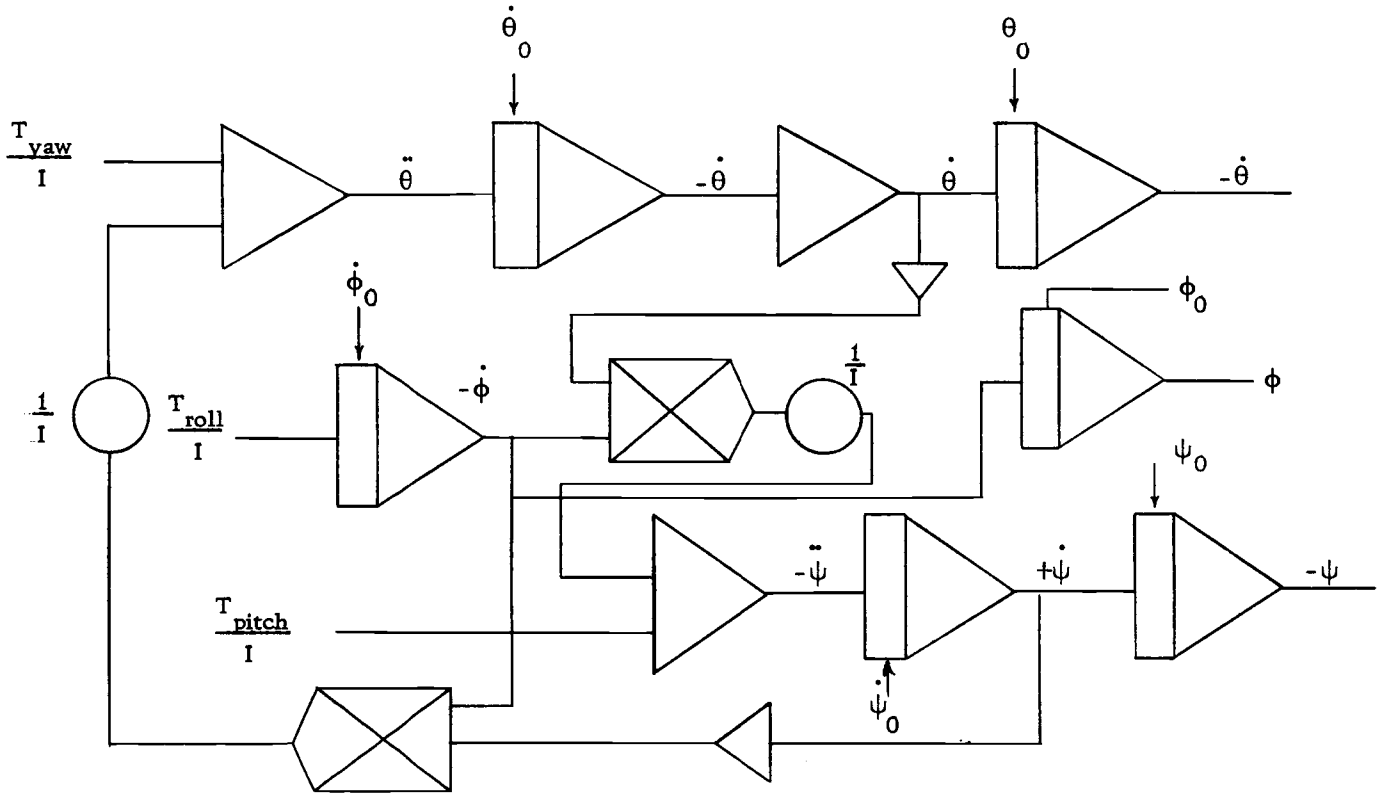

Figure 6. Analogue scheme of payload dynamics.

V. CONSIDERATIONS ABOUT CONTROLLERS

At this point in our discussion we will introduce a device which presents a nonlinearity with interesting aspects to study. The valve modulation circuit is designed to perform a variation of pulse rate and pulse width in a nonlinear manner, in order to produce the main thrust proportional to the input signal. With its addition we obtain low limit cycle rates and low susceptibility of the system to noise (6, 13).

A number of forms of control logic have been devised for use with reaction jet controllers in an effect to achieve some approximation to linear or proportional control. The simplest of these are (1) the pulse rate modulation and (2) pulse width modulation. In the first case, control torque pulses of constant width are commanded to recur at a rate proportional to a control signal which may be attitude error or vehicle, rate-damped, attitude error. The major disadvantage of this logic is the high pulse repetition rate at large errors which leads to an excessive wearing of valves. We would obtain more efficiency in fuel use by simply leaving the control jets on. In the second case, control torque pulses are commanded to recur at a fixed rate, the width of these pulses being proportional to the control signal. The disadvantage of this scheme is the repeated operation of the thrusters even at small errors when it would be preferable to leave them off.

More sophisticated schemes attempt to relieve this disadvantage through additional data processing. One such scheme, due to R. A. Schaefer (1962) is known as the pulse ratio modulator. The control logic is shown of the Figure (7a). The variable $x(t)$ shown in that figure is a function of the rate-damped, attitude error signal. It must range between 0 and ± 1 and is often taken in the form shown in the Figure (11b). In operation, the control logic moves around the flow graph of Figure (7a), turning the jet valves on long enough for the integral of $(1 - x(t))$ to accumulate T_{min} then turning the jets off long enough for the integral of $x(t)$ to accumulate to t_{min}.

Clearly if the control signal remains within the dead zone in the Figure (7b) the jets would remain continuously off, and if the control signal remains in the saturated regions of that figure the jets would remain continuously on. For intermediate values of the control signal, the control jets are pulses on and off. The pulse width, pulse rate, and duty ratio all vary with the control signal. If $x(t)$ is treated as quasi stationary, the operating characteristic are:

$$\text{Pulse width} = t_{on} = \frac{T_{min}}{1 - x}$$

$$\text{Pulse rate} = \frac{1}{t_{on} - t_{off}} = \frac{1}{T_{min}} x(1-x) \qquad (21)$$

$$\text{Duty ratio} = \frac{t_{on}}{t_{on} - t_{off}} = x$$

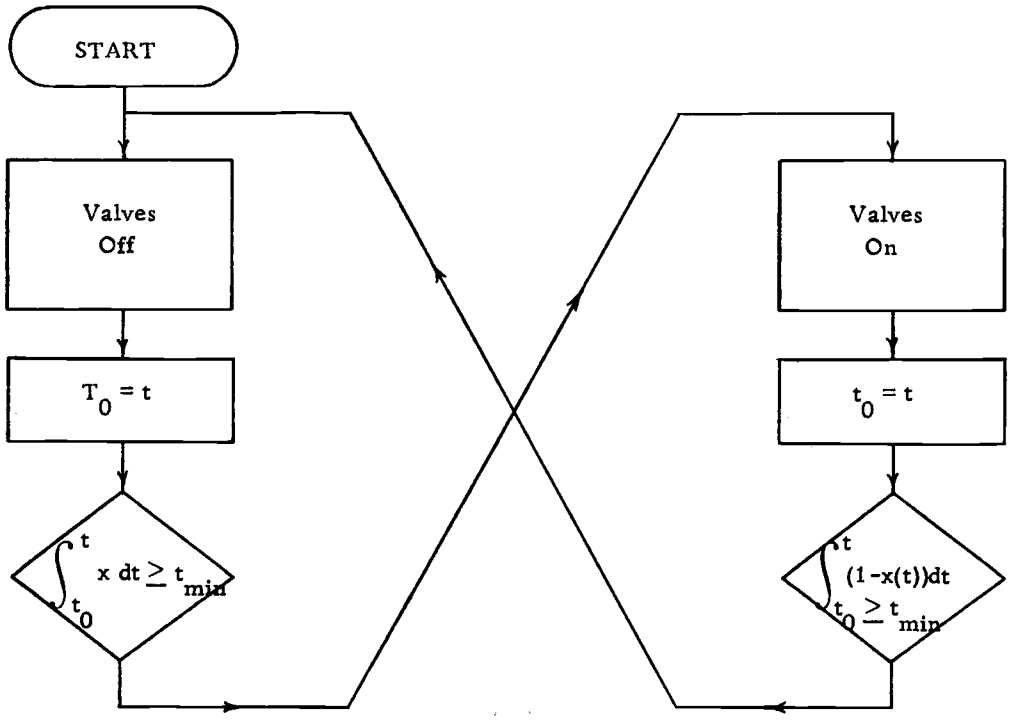

Figure 7a. Modulator logics.

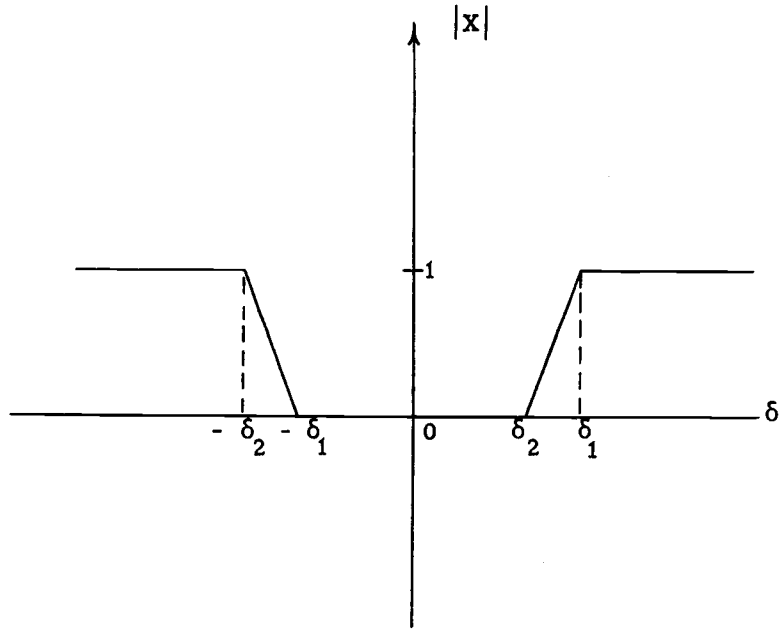

Figure 7b. Plot of X as a function of the error signal.

The variable x thus measures directly the duty ratio of the control history.

If we consider Figure (8) which represents the block diagram of the rocket nozzle valve, another nonlinear device, we can see that our nonlinear element contains hysteresis and dead band.

The hysteresis effect was computed from a description of function techniques (19). The low, level, limit cycle produced by this phenomenon, depends on the hysteresis to magnitude ratio of the thruster assembly. Two types of hysteresis are present in the system: electropneumatic in the input of the solenoid actuator and fluid in the valve thruster.

Studies have been made to show that the electropneumatic hysteresis is divided approximately 2/3 in the magnetic circuit and 1/3 in the mechanical members of the actuator (14). The magnitude for this hysteresis is a fixed fraction of the input signal.

The second type of hysteresis appears when we have secondary flows within the chamber. This kind of phenomenon can be mostly represented by a fix width that is a fixed control pressure differential. This effect is small enough to justify it being neglected.

In our case, the control element consists of dual solenoid valves driven by biased switching amplifiers in conjunction with a source of constant thrust (cold gas under high pressure). We have four distinct

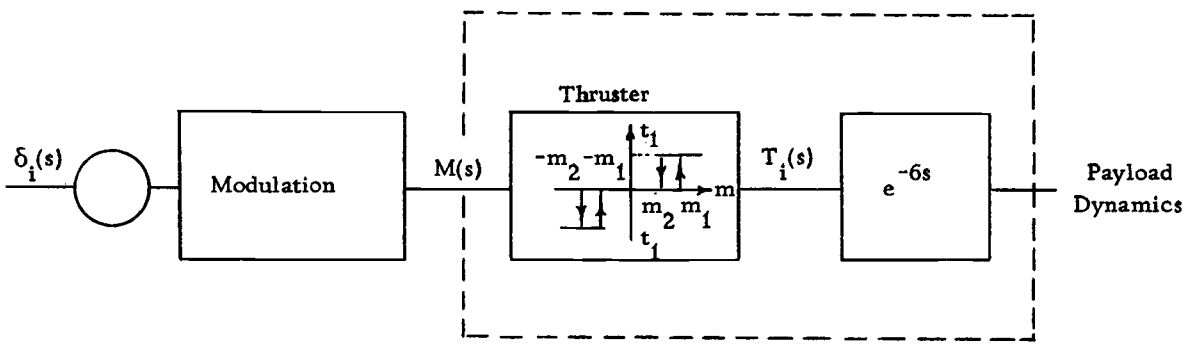

Figure 8. Diagram nozzle valve and associate devices.

modes of operation as shown in the Figure (8) and they follow the sequence shown in Table 1.

Table 1. Modes of operation of the thruster.

Modes	Direction of m(t)	Interval m(t)	T(t)	Final m
1	Decreasing	$m_2 m \; -m_1$	0	-m
2	Increasing	-m m -	-1	$-m_2$
3	Increasing	$m_1 m \; -m_2$	0	m_1
4	Decreasing	m m_2	-1	m_2

The values of the torque T_i are constant over each mode. The control element can be replaced by an open loop step function generator (21). Further, $T_i(t)$ and T(t) are identical quantities, displaced in time by the system delay. The variable T consists of a series of step functions.

In the analog thruster scheme we can observe that the output of potentiometer, Figure (9), adds to or subtracts from the input signal so that switching occurs at

$$V_{in} = |aR| \qquad V_{in} = -|aR| \tag{22}$$

The relay characteristic is achieved by summing the output of two bang-bang circuits with feedback limit units which limit at 0 and -V and 0 and V depending on the polarity of R .

With the loop b closed and R positive as the input falls from a voltage such that the output is positive (V) the effective voltage to amplifier 2 is:

$$V_{in} + bV - aR \tag{23}$$

This causes the switching when equal to zero

$$V_{in} = aR - bV \tag{24}$$

With V_{in} less than this, the output is zero and the switching to -V will occur when amplifier 1 switches

$$V_{in} = -aR \tag{25}$$

The dead band is then $2aR - bV$. In the reverse direction switching will occur at

$$V_{in} = -aR + bV \tag{26}$$

$$V_{in} = aR \tag{27}$$

The hysteresis is then bV, and the dead band decreases with increase in hysteresis. With R negative, the same overall effect is observed, but in amplifier 2 as the input voltage drops.

From the equations above it can be seen that if the dead band levels were widened to $aR - 0.5bV$ and $-aR - 0.5bV$, switching would occur at:

$$V_{in} = aR + 0.5bV - bV = aR - 0.5bV$$

$$V_{in} = -aR - 0.5bV \qquad (28)$$

$$V_{in} = -aR - 0.5bV + bV = -aR + 0.5bV$$

$$V_{in} = aR + 0.5bV$$

This would give hysteresis of bV and a dead band of $2aR$ independent of b.

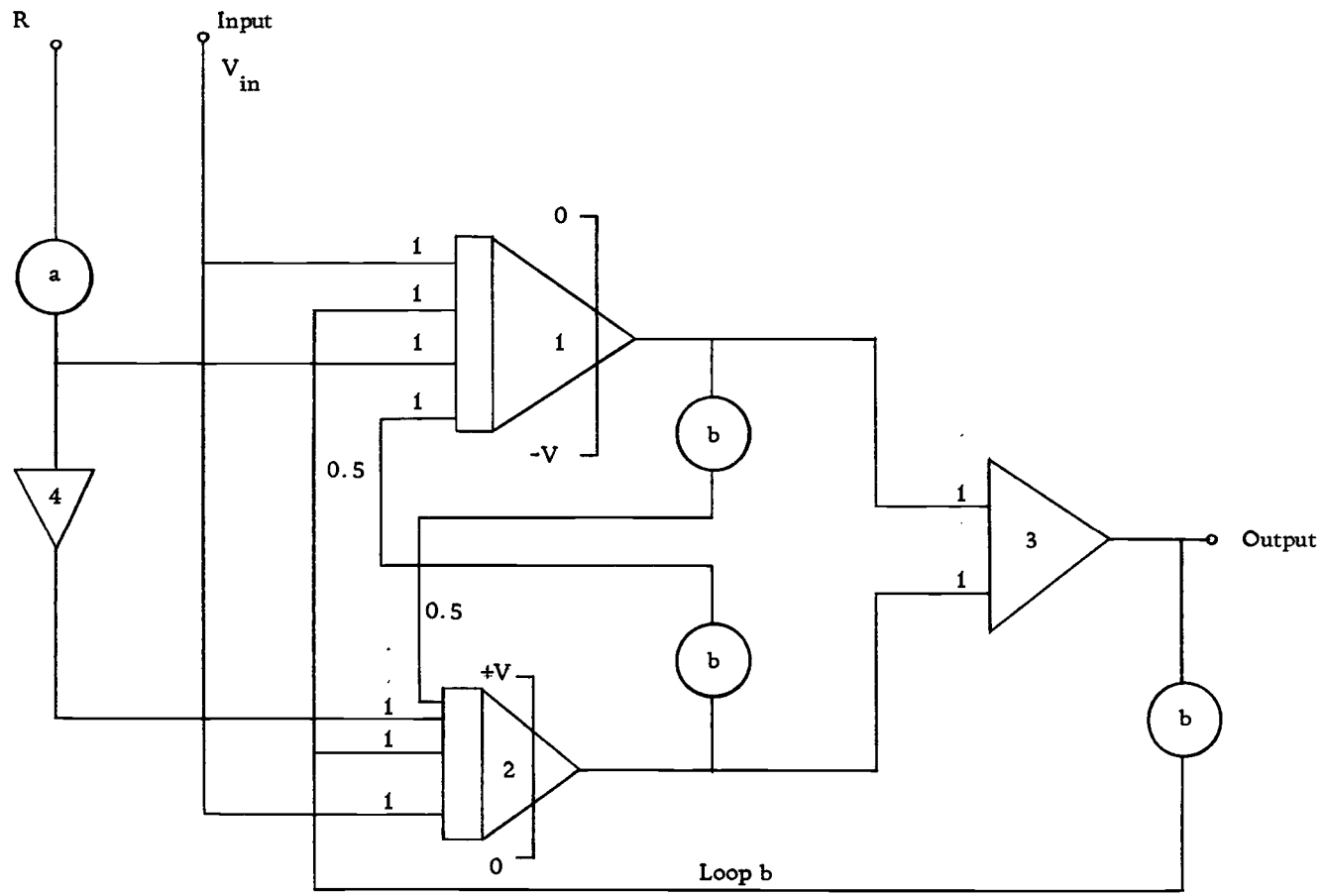

Figure 9. Solenoide valve analogue scheme.

VI. THEORETICAL ASPECTS OF THE FLUXGATE MAGNETOMETER

Aspect Sensor Type Fluxgate

This type of device is in essence an instrument which was developed at the end of the Second World War (22).

Airborne magnetometers are devices which measure the magnetic field variation in a detector in free space. Since we know the speed of the plane, this variation is recorded as a time function.

For rocketborne sensors, these variations are translated as spin information and precession angle.

The method used to acquire the information from a flux gate magnetometer is to put into the field under observation a high permeability core coil fed by a sinusoidal current able to saturate the magnetic core. The electromotive force produced by the time variation of the flux vector in the core with respect to a second coil feeds an electronic circuit where the shape of the wave is analyzed; as a result we have the magnitude of the field under test.

The behavior of such a saturated inductor may be understood if we consider that the flux density B produced in a magnetic material by a field H is an odd function of the field H. Analytically, and considering the hysteresis negligible, the above can be expressed by:

$$B = b_1 h + b_3 h^3 + b_5 h^5 + \cdots b_{n+1} h^{n+1} \qquad (29)$$

where the coefficients b_i ($i = 1, 3, 5, \cdots$) are determined by the core shape.

If we consider

H = unknown field in Oersted

H_0 = applied field in Oersted

p = two π times the frequency of H_0

we will have:

$$h = (H_0 \cos(pt) - H)\ O_e \tag{30}$$

Using the value of H in the Equation (30), substituting into the Equation (35), and developing the result in a binomial series expressed in terms of sin and cos; we may produce the following expressions:

$$B = B_0(H_0, H) + B_1(H_0, H)\cos(pt) + B_2(H_0, H)\cos(2pt) + B_3(H_0, H)\cos(3pt)\cdots \tag{31}$$

In this equation, the terms $B_i (i = 0, 1, 2, 3, \cdots)$ with i's even are odd functions of H_0 .

The electromotive force per turn in the coil will be:

$$e = 10^{-8} A \frac{dB}{dt} \text{ volts} \tag{32}$$

where A is the effective area of the section of the core.

Substituting the value of B in the Equation (32) the resulting expression is:

$$e = 10^{-8} A[pB_1 \sin(pt) + 2pB_2 \sin(2pt) + 3pB_3 \sin(3pt) + \cdots] \qquad (33)$$

As any coefficient of B is a function of H we can use any combination of them in order to express the detection. We can also use the properties of odd and even functions to construct multiple detector elements, able to separate the odd harmonics from the even ones. In general, this type of magnetic device, used as attitude sensor for scientific payloads, satellites, and autopilot remote compasses for planes, uses only one frequency, the second harmonic. More sophisticated systems are wide-band detectors in order to handle more energy. Such systems are complex because their electronic circuits must be designed with coherence of phase and amplitude among the harmonics.

The single frequency system has a low requirement of energy and its electronic design is simple. This enhances its production at low cost (22).

Analysis of Some Particular Probe Types

For the probe of Figure 10a in the presence of a field H_x, the voltage induced in the secondary due to a periodic excitation voltage e_p of odd symmetry which drives the core well into saturation, twice each excitation period is:

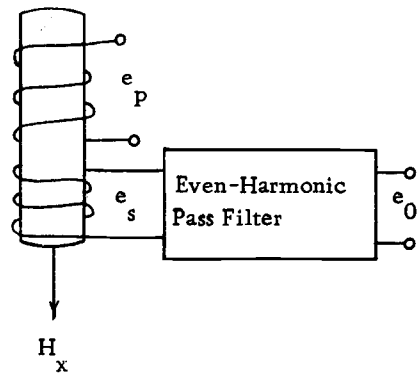

(a)

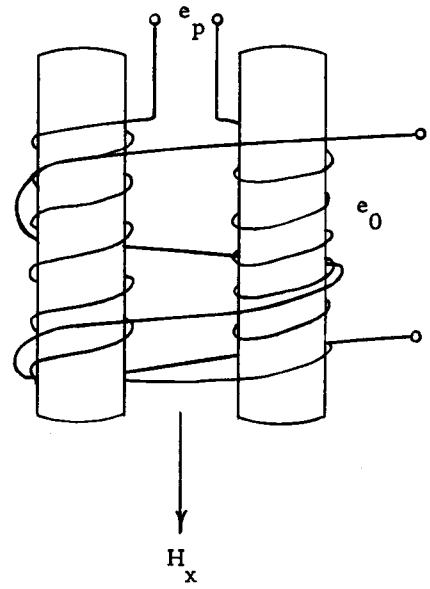

(b)

Figure 10. Some probe types.

$$e_s = NA(dB/dH)(dH/dt) \times 10^{-8}$$
$$= NA(dH/dt) \times 10^{-8}[(\mu_d)_0 + \delta H(\mu'_d)_0 + \cdots] \quad (34)$$

for $0 < t < T/2$, and

$$e_s = -NA(dH/dt) \times 10^{-8}[(\mu_d)_0 - \delta H(\mu'_d)_0 + \cdots]$$

for $T/2 < t < T$, where

N = number of output winding turns

A = core area

dH/dt = excitation field

μd = dB/dH

δH = perturbation in H within the core due to the presence of the ambient field

$(\mu_d)_0$ = dB/dH for H = 0

(μ'_d) = d^2B/dH^2 for H = 0

A perturbation in B is substituted for the perturbation in H giving

$$e_s = NA(dH/dt) \times 10^{-8}(\mu_d \frac{\delta B}{\mu_d} \mu'_d + \cdots) \quad (35)$$

for $0 < t < T/2$, and

$$e_s = -NA(dH/dt) \times 10^{-8}(\mu_d - \frac{\delta B}{\mu_d}\mu'_d + \cdots) \quad (36)$$

for $T/2 < t < T$. The subscript of μ_d and μ'_d terms have been dropped for the convenience.

The filter of Figure 10a removes odd harmonics of e_s. By taking one half the sum of corresponding terms of Equations (35) and (36), the result is the even harmonic portion of e_s defined over the entire period. This function is approximated by the first two terms for small ambient fields giving

$$e_o = NA(dH/dt) \times 10^{-8} \frac{\delta B}{\mu_d} \mu'_d \tag{37}$$

for $0 < t < T$.

The dH/dt terms related to the excitation voltage by

$$dH/dt = \frac{e_p \times 10^8}{AN_p \mu_d} \tag{38}$$

where N_p is the number of excitation winding turns, and the perturbation δB may be expressed as

$$\delta B = \mu_a H_x \tag{39}$$

where μ_a is the apparent or effective permeability of the rod-shape core to the field H_x.

Substituting (38) and (39) into (37) gives

$$\begin{aligned} e_o &= e_p(N/N_p)\mu_a(\mu'_d/\mu_d^2)H_x \\ &= e_p(N/N_p)\mu_a F_H H_x \end{aligned} \tag{40}$$

where $F_H = \mu'_d/\mu_d^2$ (32).

For the element design of Figures 10B and 11a, the odd harmonic filtering is accomplished by the bucking action of the induced voltages on the opposite sides of the probe. These induced voltages are given by (35) and (36), and the output is given by (37). If μ_a is defined for each section of the core

$$e_o = e_p(N/N_p)2\mu_a F_H H_x \tag{41}$$

The apparent permeability is related to the ballistic demagnetization factor K by

$$\mu_a = \frac{\mu_d}{1 K\mu_d} \tag{42}$$

and when K is small enough, (41) may be written as

$$e_o \tilde{=} e_p(N/N_p)2(\mu'_d/\mu_d)H_x \tag{43}$$

for a ring core probe (25)

$$K \tilde{=} 3(\sqrt{A}/M_\ell)^{1,6} \tag{44}$$

where M_ℓ is the core mean length and A is the cross-sectional area.

If for the configuration of Figure 11b the permeability is assumed to be isotropic, the voltage induced in the output coil is

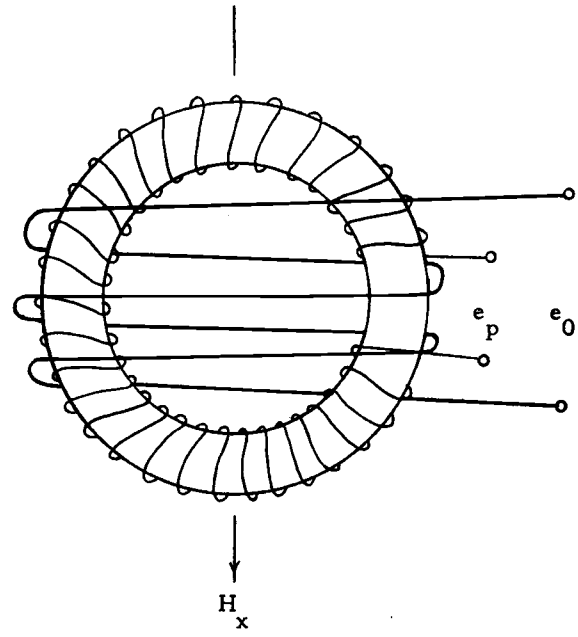

(a)

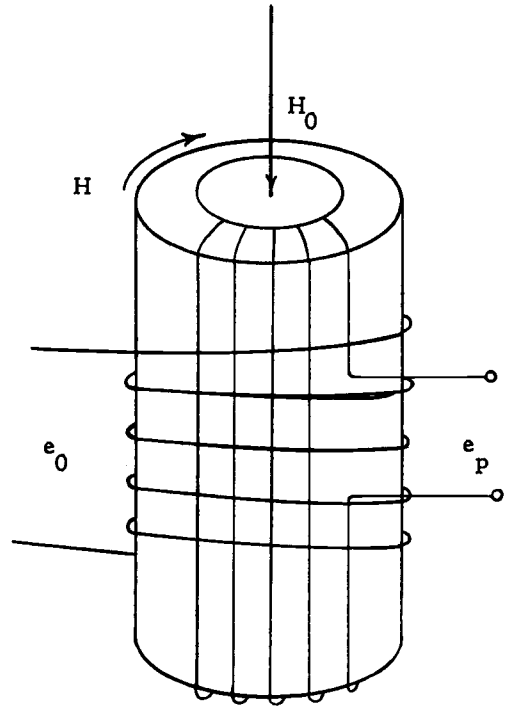

(b)

Figure 11. Some probe types.

$$e_o = NA(dH\phi/dt) \times 10^{-8}(dB_x/dH\phi) \tag{45}$$

and

$$\begin{aligned} dB_x/dH_\phi &= d(\mu_a H_x)/dH_\phi \\ &= H_x \frac{\mu'_d}{(1 - K\mu_d)^2} \end{aligned} \tag{46}$$

Substituting (46) and (45) and using (38) gives

$$e_o = e_p(N/N_p)H_x \frac{\mu'_d}{\mu_d(1 + 2K\mu_d + K^2\mu_d^2)} \tag{47}$$

For cores having large length-to-diameter ratios, the Equation (47) differs from (43) only by a factor of two. Thus, under assumption of isotropy in μ_d, the derived outputs from the three probe types have the same form. The output e_o reaches the maximum, and the amplitude of the maximum is linearly proportional to the field H_x (23).

To optimize the sensitivity to H_x the product $\mu_a F_H$ should be made as large as possible and the excitation function so designed that at the time this maximum is reached, e_p is also a maximum. It can be seen experimentally that the output pulse from a practical probe is formed only after the core is driven into the saturation, past what might normally be regarded as the knee of the hysteresis loop. This means that if the analytic model is correct, $\mu_a F_H$ reaches a maximum in the saturation region. It has been observed that the output pulse width is on the order of 10 to 20 μs when the core is excited at frequencies from 0.5 kHz to 1.0 kHz. Then for a reasonably smooth

excitation voltage, e_p or dB/dt may be considered constant at the instant the output pulse is formed. Substituting

$$e_p = N_p A \times 10^{-8} dB/dt \tag{48}$$

into (41) gives

$$e_o = 2NA \times 10^{-8} (dB/dt) \mu_a F_H H_x \tag{49}$$

for the time period during which the pulse is formed, and e_o is essentially zero elsewhere. Integrating (49) with respect to time we have

$$\int_{t_i}^{t} e_o dt = 2NA \times 10^{-8} H_x \int_{B_i}^{B} \mu_a F_H dB \tag{50}$$

which shows that the volt-seconds of the output pulse is a constant of the core parameters and H_x, and is independent of the excitation function. That is, one may obtain a large amplitude narrow pulse or a smaller amplitude fatter pulse. Also, Equation (50) shows that following the volt-seconds generated by integration from B_i to B_{max} during one half-period (assuming the maximum of $\mu_a F_H$ lies within $B_i < B < B_{max}$) there is another pulse of opposite sign generated when the cycle reverses and the integration is from B_{max} to B_i. The signs of F_H and μ_a do not change, but since the limits on the right-hand integral of Equation (50) are reversed, its sign also changes.

The sign for left-hand integral may change if e_o changes polarity.

When we consider the overall system the sensitivity is limited by the high impedance input of the detector. If we have a constant input impedance on the detector, the sensitivity increases with the core length and is affected a little by the section.

The length of the core must be such that the magnetic noise in the inductor produced by random movings of the device into the geomagnetic field as well as the approximations of magnetic masses be greater than the noise due the detector.

Another source of noise that limits the sensitivity of the instrument is the Barkhausen Effect (14). This effect is very small when we compare it with the total noise of the system in flight.

Using the flux-gate magnetometer as a rocket aspect sensing device, the total magnetic (geomagnetic) field intensity at any point is available from a magnetic field model (5). When sound rockets have been flown with sets of flux-gate magnetometers it has frequently been found that measures of field values differ considerably from the theoretical ones. This appears to be due to the fact that the rocket becomes magnetized during the launch.

During the course of one spin cycle, the rocket axis remains approximately fixed in space. Hence, outputs of the two transverse magnetometers should be sinusoidal, and their maximum outputs should be the current values of the horizontal field component.

When there exists a permanent dipole along the magnetometer direction, its output is sinusoidal, but it is not centered about zero milligauss. The difference between the central position of the magnetometer output and zero reference level is the value of the dipole (6).

Using the data from both magnetometers we can establish the horizontal dipole P_h. The theoretical total field F_t is known from the model. To get the permanent dipole P_x of the magnetometer along the payload axis, we first calculate the theoretical reading $F_{xt} = (F_t^2 - P_h^2)$ then

$$P_x = F_{xm} - F_{xt} \tag{51}$$

VII. SIMULATION MODEL FOR THE MAGNETOMETER

In order to characterize the rotation we will use the three non-orthogonal Euler Angles, yaw, pitch and roll, which permit the reference frame to be aligned by successive rotations with the body fixed frame. Consider one frame fixed in the payload and other fixed in the earth but with the same translation of the center of mass of the payload.

Use for this situation three reference frames:

a. The fixed system, X, Y, Z, connected to the center of mass of the payload. It has the Z-axis in the same direction as the angular momentum ($\vec{\sigma}$). This is a very convenient direction to be chosen, since it has the absence of external torques and it will stay fixed in the space.

The direction of the momentum angular can be described by the angle β, see Figure 13.

b. The second system $X_c Y_c Z_c$ constrained to the payload which has its Z_c axis in the direction of the longitudinal axis of the payload. X_c is such that the longitudinal axis of the magnetometer lies in the plane $X_c - Z_c$.

c. The third will be x, y, z fixed in the payload where z has the same direction as the longitudinal axis of the magnetometer.

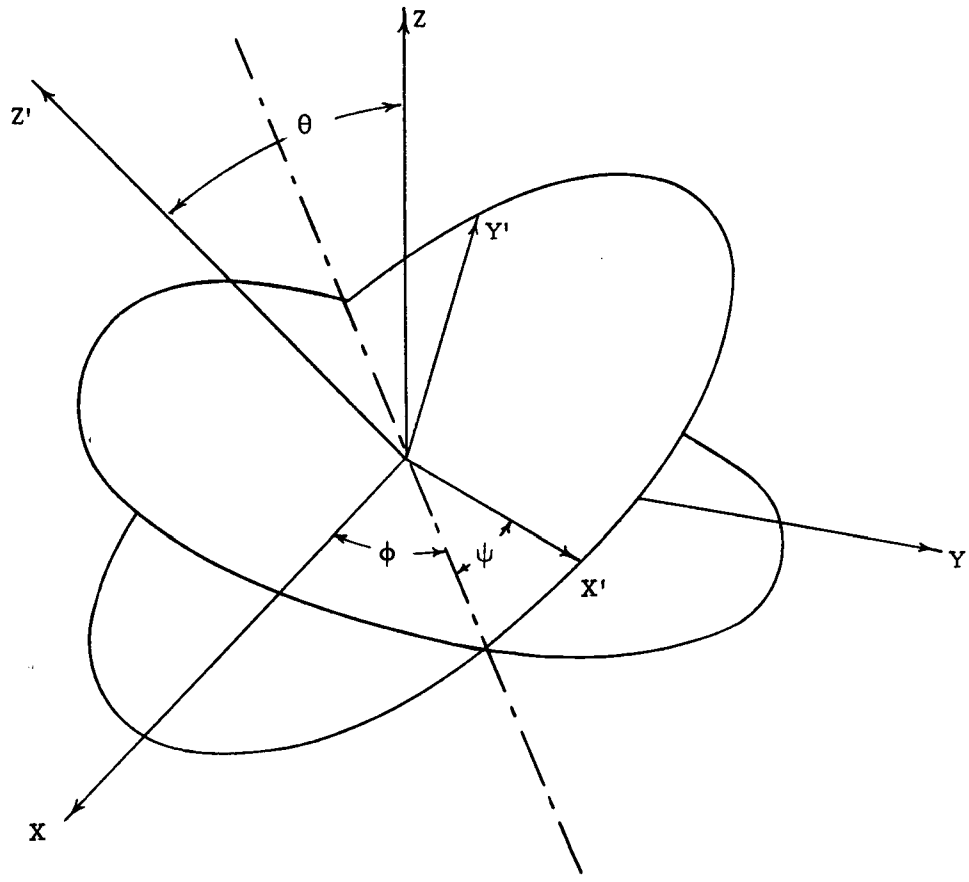

Figure 12. Eular angles (ϕ , θ , ψ).

The Euler angles (ϕ , θ, ψ) will be used to specify the payload attitude with respect to the fixed system X, Y, Z .

A ridig body rotating with respect to its center of mass is described by Euler equations. These equations can be represented in vectorial form as:

$$\dot{\vec{\sigma}} = \frac{d}{dt} J\vec{\omega} \tag{51}$$

Expressing J and $\vec{\omega}$ in the system of reference $X_c Y_c Z_c$ the time derivative of $\vec{\sigma}$ will be:

$$\frac{d\vec{\sigma}}{dt} = J\vec{\omega} + \vec{\omega} \times J\vec{\omega} = \vec{0} \tag{52}$$

where J is the moment of inertia tensor and $\vec{\omega} = \omega_1 X_e + \omega_2 Y_c + \omega_3 Z_c$.

Considering now that $X_c Y_c Z_c$ are a set of inertial axes the Euler equations are:

$$\begin{aligned} N_1 &= I_1\dot{\omega}_1 + \omega_2\omega_3(I_3 - I_2) \\ N_2 &= I_2\omega_2 + \omega_1\omega_3(I_1 - I_3) \\ N_3 &= I_3\omega_3 + \omega_1\omega_2(I_2 - I_1) \end{aligned} \tag{53}$$

To avoid unnecessary complications we can assume that the payload is in the unpowered part of the flight and its altitude is above 40 miles where the pressure is sufficiently low to cause negligible aerodynamic drag. Then $N = 0$, and considering the payload axisymmetric $I_1 = I_2 = I$, we can write:

$$
\begin{aligned}
I\dot{\omega}_1 &= \omega_2\omega_3(I - I_3) \\
I\dot{\omega}_2 &= \omega_1\omega_3(I_3 - I) \\
I_3\dot{\omega}_3 &= 0
\end{aligned}
\tag{54}
$$

Now $\dot{\phi}, \dot{\theta}, \dot{\psi}$ are angular velocity components of the payload on the Z_c axis, on the node line, and on the Z axis respectively. We can easily arrive at an expression for the components of ω in the system $X_c Y_c Z_c$.

$$
\begin{aligned}
\omega_1 &= \dot{\phi}\sin\theta\sin\psi + \dot{\theta}\cos\psi \\
\omega_2 &= \dot{\phi}\sin\theta\cos\psi - \dot{\theta}\cos\psi \\
\omega_3 &= \dot{\phi}\cos\theta + \dot{\psi}
\end{aligned}
\tag{55}
$$

Considering the precession angle constant, $\dot{\theta} \tilde{=} 0$ and the above equations become:

$$
\begin{aligned}
\omega_1 &= \dot{\phi}\sin\theta\sin\psi \\
\omega_2 &= \dot{\phi}\sin\theta\cos\psi \\
\omega_3 &= \dot{\phi}\cos\theta + \dot{\psi}
\end{aligned}
\tag{56}
$$

Then taking ω_1 or ω_2 from (56) and substituting in Equations (54) and using the hypothesis that $\ddot{\phi} = 0$ and $\dot{\theta} \tilde{=} 0$ we get

$$
\omega_3 = \frac{I}{I - I_3}\dot{\psi}
$$

Then:

$$\frac{I}{I - I_3}\dot{\psi} = \dot{\phi}\cos\theta + \dot{\psi}$$

Dividing this expression by $\dot{\psi}$ we have

$$\frac{I}{I - I_3} = \frac{\dot{\phi}}{\dot{\psi}}\cos\theta + \frac{\dot{\psi}}{\dot{\psi}} = \left(\frac{I}{I - I_3} - 1\right)\frac{1}{\cos\theta} = \frac{\dot{\phi}}{\dot{\psi}}$$

or

$$\frac{\dot{\psi}}{\dot{\phi}} = \left(\frac{I}{I_3} - 1\right)\cos\theta = \frac{\omega_s}{\omega_p} \tag{57}$$

where ω_s = spin rate and ω_p = precession rate.

The precession angle is small and $I >> I_3$. The ratio between the angular speed of spin and precession rate can be written:

$$\omega_s \tilde{=} \omega_p \frac{I}{I_3} \tag{58}$$

As $I >> I_3$, always $\omega_s >> \omega_p$. By integration we can obtain the Euler angles ϕ and ψ.

$$\begin{aligned} \phi &= \phi_0 + \omega_p t \\ \psi &= \psi_0 + \omega_s t \end{aligned} \tag{59}$$

To relate the movements of the payload and the output of the magnetometer we must know the value of the geomagnetic field measured by the sensor. This relationship, i. e., the output of the sensor can be described by:

$$b = B_0 \cos\varepsilon\,(t) \tag{60}$$

where b is the output voltage, B_0 is the magnitude of the field and $\varepsilon(t)$ is a function of several angles.

Now we shall express $\varepsilon(t)$ in terms of these angles. The best way to do this task is to express the unit vectors $\vec{Z}$ and $\vec{B}$ on the same reference system and obtain $\cos(\varepsilon)$ through the scalar product between them. Let's choose the reference system $X_c Y_c Z_c$ for which

$$\vec{Z} = \sin\delta X_c + \cos\delta Z_c \tag{61}$$

In the referencial X Y Z

$$\vec{B} = \sin\beta\, X + \cos\beta Z \tag{62}$$

which when transformed to the chosen reference system will give

$$\begin{aligned}\vec{B} = {} & (\cos\beta\sin\theta\sin\psi + \sin\beta\cos\phi\cos\psi - \sin\beta\sin\phi\cos\theta\sin\psi)X_c \\ & + (\cos\beta\sin\theta\cos\psi - \sin\beta\cos\phi\sin\psi - \sin\beta\sin\phi\cos\theta\cos\psi)Y_c \\ & + (\cos\beta\cos\theta + \sin\beta\sin\phi\sin\theta)Z_c\end{aligned} \tag{63}$$

Operating the scalar product between Z and B

$$\vec{Z}\cdot\vec{B} = \cos\varepsilon$$

which through the expressions (61), (62), and (63) will give the expected equation.

$$\begin{aligned}\cos(\varepsilon) = {} & \sin\delta\cos\beta\sin\theta\sin\psi + \sin\delta\sin\beta\cos\phi\cos\psi \\ & - \sin\delta\sin\beta\sin\phi\cos\theta\sin\psi + \cos\delta\cos\beta\cos\theta \\ & + \cos\delta\sin\beta\phi\sin\theta\end{aligned} \tag{64}$$

If we do not consider the variations of the amplitude resulting from the variations of B, the output signal from the magnetic sensor will be a function of $\cos\varepsilon$. This relation is similar to the expression given for the $\cos\varepsilon$ in the reference 35. The differences lie in the different orientation of the axis and the different symbols for the Euler angles.

Let's analyze the function given by Equation (64) in order to determine the necessary parameters.

Let's define

$$a = \cos\beta\sin\delta\sin\theta$$

$$c = \sin\beta\sin\delta$$

$$d = c\cos\theta$$

$$e = \cos\beta\cos\delta\cos\theta$$

$$g = \sin\beta\cos\delta\sin\theta$$

which permits us to rewrite Equation (64) in a close form:

$$\cos\varepsilon = (e + g\sin\phi) + (c\cos\phi)\cos\psi + (a - d\sin\phi)\sin\psi \qquad (65)$$

Using some trigonometric relationship we can write:

$$\cos\varepsilon = (e + g\sin\phi) + a\sin\psi + \frac{c+d}{2}\cos(\psi + \phi) + \frac{c-d}{2}\cos(\psi - \phi) \qquad (66)$$

This equation related with the fact that $\omega_s >> \omega_p$ allows the formulation of a fair image of the behavior of $\cos\varepsilon$. For $\theta << 1$,

$$\frac{c-d}{2}\cos(\psi - \phi) \tilde{=} 0$$

This means that the output will be a sinusoid with amplitude close to $\frac{c - d}{2}$ and frequency $(\omega_p + \omega_s)$ plus another term $(e + g \sin\phi)$ with a very low frequency which represents the average level of the output.

For the purpose of simulation, in order to obtain the output suitable for application on the whole system, we must use an analogue set up of the Equation (66).

The present analysis can be useful in determining the optimum angle of the sensor, to obtain simultaneously acceptable amplitudes for spin and precession signals.

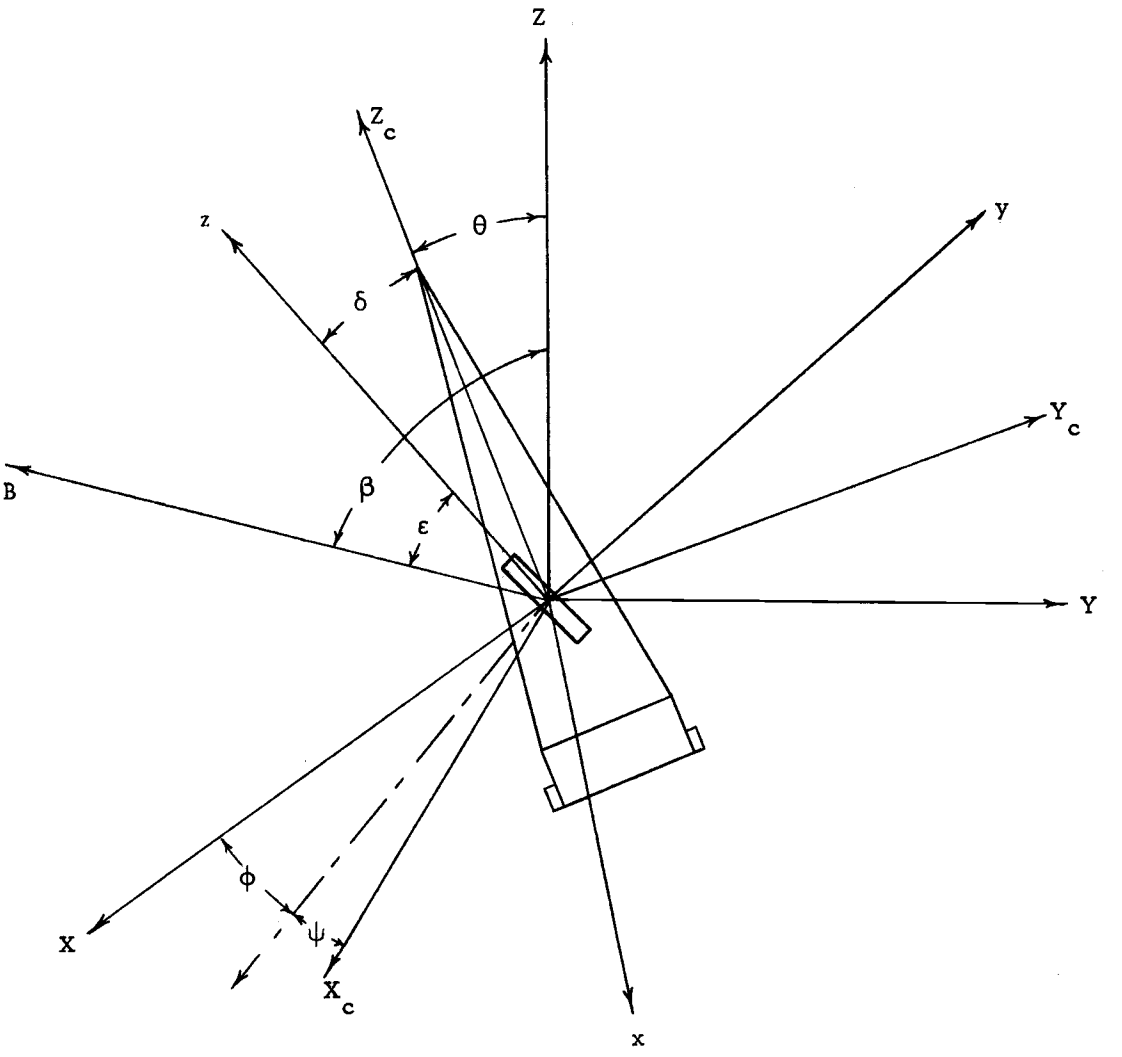

Figure 13. Reference frames used in the development of the magnetometer model.

VIII. CONCLUSIONS

The approach presented has several advantages in terms of cost and practicality since mechanical sensing devices were replaced by solid state circuitry. A study was carried out in order to analyze the possibilities for the use of only one magnetometer as a secondary source to obtain the error signals.

We should expect some problems with the earth shine. Pitch error signals obtained from $+S_{13}$ and $-S_{13}$ solar cells, when reflected light from earth hits the either cell, will be in error and the result can be as large as 20^{o} (6). To compensate for such error we can use another pair of solar cells with a narrower field of view (5). An exact cancellation of the earth shine effect is not possible but if the error lies inside a range of 10^{o} we can be sure that the sun will enter in the field of view of the payload sensing devices.

Technical details, such as: solar cell masking in order to obtain the desired output law, the circuitry to perform the modulation of the error signals, were not discussed. These details are specific to a particular mission but do not affect the general nature of the total system.

The simulation model for the magnetometer permits us to study the advantages of using one or two such sensors. Depending on the latitude where the experiment will be carried, this model can give a

very good idea about the output of the magnetometer for different conditions. This permits locating the sensor at the best angle with respect to the principal axis of the payload.

BIBLIOGRAPHY

1. Aseltine, J. A. Peaceful Uses of Automation in Outer Space. Proceedings of the First I. F. A. C. Symposium on Automatic Control in Peaceful Uses of Space. Stavanger, Norway, 1965. New York, Plenum Press, 1966.

2. Amarante, J. A. A. Um Metodo Para a Determinaçao da Atitude de Foguetes em Voo Livre Atraves oUso de Sensores Magneticos. C. N. A. E. LAFE-057. 1967.

3. Atran, L. Analysis of a Nonlinear Control System for Stabilizing a Missile. IRE Trans. on Automatic Control. November, 1957.

4. Borisenko, A. I. and I. E. Terapov. Vector and Tensor Analysis with Applications. N. J. Englewood Cliffs, Prentice-Hall, Inc., 1968.

5. Cahill, L. J., Jr. A Study of Outer Geomagnetic Field. IEEE. Trans. on Nuclear Science, Vol-NS10, July, 1966.

6. Charles, D. Howard, J. Innes Daphne and Dolan Mansir. Space Vehicle Attitude Studies. A. F. C. R. L. 68-0610. November 1968 Instrumentation Papers.

7. Chisel, D. M. and R. K. Rose. Fluidic Proportional Thruster System for Rocket Application. ASME Paper 68-WA/FE 32, for Meeting December, 1968.

8. Collette, J. G. R. Analysis and Design of Space Vehicle Flight System. N. A. S. A. CR-830, July 1967.

9. Daniel, I. Gordon, H. Lundten Richard, A. Chiarodo Roger and H. Helms Horace, Jr. A Flux-Gate Sensor of High Stability for Low Field Magnetometry. IEEE. Trans. on Magnetics, Vol. 13 Mag 4, no. 3, September, 1968.

10. Fleischer, H. A. Scheme to Desaturate Accumulated Gravity Gradient Momentum. The Bendix Corporation Navigation and Control Division, Report MT-15, 112.

11. Fleischer, H. A. New Method of Orbit Attitude Determination Bendix Technical Journal, Vol. 1, No. 1, Spring, 1968.

12. Glass, M. S. Principles of Design of Magnetic Devices for Attitude Control. B. S. T. J. May-June 1967.

13. Giacomo, Porcelli. Large Angle Attitude Control of a Spinning Space Body. IEEE. Trans. on Automatic Control. December, 1969.

14. Gorgan, D. I. A Experimental Study of Barkhausen Noise in Nickel-Iron Alloys. Rev. Mod. Phys. Vol. 25, No. 1. 1967.

15. Greer, H. and D. J. Griep. Dynamic Performances of Low Thrust Cold Gas Reaction Jets in Vacuum. Journal of Spacecraft and Rockets, Vol. 4, No. 8. August, 1967.

16. Greesite, A. L. Analysis and Design of Space Vehicle Flight Control System. N. A. S. A. CR 820 July, 1967.

17. Hansen, Q. M., E. A. Gabris, M. D. Pearson and B. S. Leonard. Gyroless Solar Pointing Attitude Control System for Aerobee Sound Rocket. Journal of Spacecraft and Rockets. Vol. 4, No. 11, November, 1967.

18. Hazell, J. F., P. E. G. Cope, I. F. M. Walker. Development and Operation of Stabilized Skylark Rocket. Journal of Spacecraft and Rockets. Vol. 5, No. 4, April, 1968.

19. John, E. Gibson. Nonlinear Automatic Control. New York. McGraw-Hill Co., 1963.

20. Instrument Society of America Multilingual Dictionary of Automatic Control Terminology. Pittsburgh, D. T. Broadbent Instrument Society of America, 1967.

21. Kumar, K. S. P. On Optimal Stabilization of Satellite. IEEE. Trans. on Aerospace and Electronic Systems. Vol. AES-1, No. 2, October, 1965.

22. Langill, A. W., Jr. Automatic Control Systems Engineering. New Jersey, Englewood Cliffs, Prentic-Hall, Inc. 1965.

23. Ling, S. C. A Flux-Gate Magnetometer for Space Application. Cornell University Center of Radiophysics and Space Research. N. Y. Quart. Status Report to N. A. S. A. CRSR124 N. A. S. A. contract NaSr-46 June 1, 1962.

24. Lowi, A. Spacecraft Jet Reactional Control. Aerospace Corporation, TOR-649 (5560) 10. July, 1962.

25. Mattis, Daniel C. The Theory of Magnetism. 2nd. ed. New York. Harper & Row Inc. 1965.

26. Max, M. F. Design Aspects of Attitude Control Systems. IRE Trans. on Attitude Control, Frebruary, 1961.

27. Miller, J. E. Navigation Guidance and Control. London, Maidenhead, Technivision Limited. 1966.

28. Rasmussen, R. O., A. Lanzaro, N. F. Sinnott and D. R. Schaefer. Attitude Control for Spinning Sound Rockets. Report from Technical Products Division Whittake Corporation, Chatsworth, California.

29. N. A. S. A. Final Report on Rely Program. S. P. 76.

30. Peter, W. L. and H. Karl Bouvier. Attitude Control on Non-Rigid Spacecraft. Astronautics and Aeronautics Vol. 9, No. 5 May, 1971.

31. Schaefer, R. A. A. New Pulse Modulator for Accurate DC Amplifier with Linear or Nonlinear Devices. IRE Trans. on Instrumentation. Vol. 1, 2, No. 2, September, 1962.

32. Stanley, U. M. An Analytic Model for the Flux-Gate Magnetometer. IEEE Trans. on Magnetics, Vol-Mag-3, No. 3, September, 1967.

33. Sorensen, J. A. A Magnetic Attitude Control System for Axis Simetric Spinning Spacecraft. Journal of Spacecraft and Rockets. Vol. 8, No. 5, May, 1971.

34. Thomas, W. R. Sub Orbital Probes. Royal Society. London. Proc. Ser. A. Vol. 308, No. 1493, January 7, 1969.

35. Young, G. R. and J. D. Timmons. On the Use of Magnetometer to Determine Angular Motion of a Spinning Body in Regular Precession. N. A. S. A., TN D-2284, May, 1964.

36. Williams, P. C. and S. W. Noble. The Fundamental Limitation of the Second Harmonic Type of Magnetic Modulator as Applied to the Amplification of Small DC Signals. Proc. IEEE. Vol. 97, pt. 12, 1950.

37. Williams, A. G. A New Type of Magnetometer. Journal of Applied Physics, Vol. 33, No. 3, March, 1962.